Published in final edited form as:
Mol Pharm. 2013 October 7; 10(10): . doi:10.1021/mp400360q.

Long-Circulating Heparin-Functionalized Magnetic Nanoparticles for Potential Application as a Protein Drug Delivery Platform

Jian Zhang[†,‡,#], **Meong Cheol Shin**[†,‡,#], **Allan E. David**[§], **Jie Zhou**[‖], **Kyuri Lee**[‡], **Huining He**[†], and **Victor C. Yang**[*,†]

[†]Tianjin Key Laboratory on Technologies Enabling Development of Clinical Therapeutics and Diagnosis, School of Pharmacy, Tianjin Medical University, Tianjin 300070, China

[‡]Department of Pharmaceutical Sciences, College of Pharmacy, University of Michigan, 428 Church St., Ann Arbor, MI 48109, USA

[§]Department of Chemical Engineering, Samuel Ginn College of Engineering, Auburn University, 222 Ross Hall, Auburn, AL 36849, USA

[‖]Department of Urology, the First Affiliated Hospital, Guangxi Medical University, Nanning, 530021, Guangxi, P.R. China

Abstract

Starch-coated, PEGylated and heparin-functionalized iron oxide magnetic nanoparticles (DNPH) were successfully synthesized and characterized in detail. The PEGylation (20 kDa) process resulted in an average coating of 430 PEG molecules per nanoparticle. After that, heparin conjugation was carried out to attain the final DNPH platform with 35.4 μg of heparin/mg Fe. Commercially acquired heparin-coated magnetic nanoparticles were also PEGylated (HP) and characterized for comparison. Protamine was selected as a model protein to demonstrate the strong binding affinity and high loading content of DNPH for therapeutically relevant cationic proteins. DNPH showed a maximum loading of 22.9 μg protamine/mg Fe. In the pharmacokinetic study, DNPH displayed a long-circulating half-life of 9.37 h, 37.5-fold longer than that (0.15 h) of H P. This improved plasma stability enabled extended exposure of DNPH to the tumor lesions, as was visually confirmed in a flank 9L-glioma mouse model using magnetic resonance imaging (MRI). Quantitative analysis of the Fe content in excised tumor lesions further demonstrated the superior tumor targeting ability of DNPH, with up to 31.36 μg Fe/g tissue (13.07% injected dose (I.D.)/g tissue) and 7.5-fold improvement over that (4.27 μg Fe/g tissue; 1.78% I.D./g tissue) of HP. Overall, DNPH shed light of the potential to be used as a protein drug delivery platform.

Keywords

Magnetic targeting; Iron oxide nanoparticles; Heparin; 9L-glioma; Magnetic resonance imaging

1. Introduction

Based on Cancer Statistics,[1] 1.66 million new cancer cases and 0.58 million cancer deaths (1 in 4 total deaths) are estimated to occur in the United States in 2013. Despite several decades of effort, only modest improvement has been achieved. This is especially true for cancers in

[*]Author to whom correspondence should be addressed: Victor C. Yang, PhD., Albert B. Prescott Professor of Pharmaceutical Sciences, College of Pharmacy, The University of Michigan, Ann Arbor, MI 48109-1065, USA, Tel: 01-734-764-4273; Fax: 01-734-763-9772, vcyang@umich.edu.
[#]Authors contributed equally to this work

the brain and other nervous system (e.g., malignant gliomas),[2] which are the second most common cancer type accounting for 25% of all cancer cases. Brain tumors have ruthlessly defied all conventional therapies including surgery, chemotherapy, immunotherapy and radiotherapy. As a result, many patients with malignant brain tumors receive only symptomatic care to ease end-of-life with a median survival time of only 10-14 months.[3]

This worldwide incidence of malignant tumors resulted in vigorous and extensive attempts in utilizing a whole variety of cytotoxic agents. However, conventional administration of small molecule anti-tumor drugs encounters a host of shortcomings, such as poor efficacy and severe side effects, primarily due to their low potency and lack of selectivity towards tumor cells. To overcome these problems, the use of macromolecule drugs such as protein toxins[4-6] and siRNAs[7-9] has recently gaining increased attention. Owing to their unmatched reaction specificity and efficiency, IC_{50} of these macromolecular drugs often occurs in the "pmol" range (e.g. IC_{50} for the gelonin toxin against human glioma cells was shown to be about 15 pmol[10]). These drugs therefore are able to supersede the potency barrier by eradicating tumors at exceedingly low bio-available drug concentrations at the target site. Clinical translation of macromolecular drugs, however, has largely been prohibited, due to the low bioavailability, instability in physiological environment and, most critically, poor intracellular transportation of these agents. Nevertheless, in previous study, we demonstrated the feasibility to achieve effective intra-tumoral uptake of these toxins by covalently linking them with a cell-penetrating peptide (CPP) such as TAT peptide or low molecular weight protamine.[10,11]

Magnetic nanoparticles (MNP), specifically iron oxide-based, generally compose of a magnetite (Fe_3O_4) core coated with a polymeric shell.[12] They have been widely attempted as drug carriers to achieve simultaneous magnetically-enhanced tumor targeting and magnetic resonance imaging (MRI).[13-15] The *in vivo* biocompatibility and large surface area-to-volume ratio for drug loading render MNP ideal candidates for the so-called "theranostic" applications.[16,17] By further coating MNP with a heparin layer, we recently reported the plausibility of attaching CPP-linked large protein (β-galactosidase) to the nanoparticle surface, via electrostatic interaction between the cationic CPP and the anionic heparin molecule.[18] However, intra-arterial administration was utilized in that study due to the poor plasma half-life (less than 5 min) of heparin-coated MNP. Despite the promising clinical application, intra-arterial and particularly intra-carotid administration of MNP is one of the least preferable methods in clinical practice. The MNP aggregation under the influence of the applied magnetic field (for magnetic targeting) can cause significant embolism of the afferent vasculature. As noted, occlusion of the carotid artery, which directly supplies the normal brain parenchyma, can lead to severe neurological-sequelae. To this regard, development of a long-lasting, MNP-based platform for therapeutic proteins, suitable for both intravenous injection and magnetic targeting for the treatment of brain cancers, is of the most essential and urgent need.[19]

Here, we reported the successful development of such a system. To reach the long-circulating purpose, the starch-coated MNP was modified with an appropriate amount of the protective 20-KDa PEG chains. The PEGylation can also favor MNP a better passive targeting via the enhanced penetration effect (EPR).[20] To enable loading of the highly cationic CPP-linked protein drug in the future, PEGylated MNP was further modified with a layer of highly negatively charged heparin to yield the final product of DNPH. To further evaluate the potential application of this novel DNPH system, protamine, a highly cationic CPP, was chosen as the model drug. Protamine is clinically used as a heparin antidote to reverse the anticoagulant effect of heparin after cardiovascular surgeries due to the strong charge interaction between anionic heparin and cationic protamine, which enables the formation of the stable DNPH-protamine complex. By attempting protamine as the model

CPP-linked cationic protein drug and using a clinically relevant 9L-glioma mouse model, the prepared DNPH thus displayed a long circulating plasma half-life, low RES recognition and high efficiency for subcutaneous tumor magnetic targeting, as well as the capability for magnetic resonance imaging (MRI). Overall, the results of this preliminary study shed light of the potential of utilizing this synthesized DNPH as a promising platform for tumor selective delivery of protein therapeutics.

2. Experimental

2.1 Materials

The starch-coated magnetite (Fe_3O_4)-cored nanoparticles fluidMAG-D ("D") and fluidMAG-Heparin ("H") were acquired from Chemicell® GmbH (Berlin, Germany). Methoxyl polyethylene glycol succinimidyl carbonates (mPEG-NHS, 20 kDa) and methoxyl polyethylene glycol amine (mPEG-NH_2, 20 kDa) were commercially supplied by JenKem Technology (Texas, USA). Iron standard (1000 mg Fe/L) and Yittrium internal standard (1000 mg Fe/L) were purchased from GFS Chemicals (Ohio, USA). Slide-A-Lyzer dialysis cassette was purchased from Thermo Scientific (Illinois, USA). Lacey carbon type A copper grids were obtained from Ted Pella (300-mesh, California, USA). U-100 insulin syringes were commercially acquired from Becton Dickinson (New Jersey, USA). Protamine, heparin sodium salt (from porcine intestinal mucosa, 193 U/mg), N-hydroxysuccinimide (NHS), 1-Ethyl-3-(3-dimethylaminopropyl) carbodiimide (EDC), 4-Dimethylaminopyridine (DMAP), Ninhydrin reagent (2%, w/v), 0.1 N iodine solution, barium chloride ($BaCl_2$, 10% of w/v), dimethyl sulfoxide (DMSO), Dimethyl Formamide (DMF), BCA assay kit, sodium phosphate (mono- and di-basic), concentrated hydrochloric acid (HCl, 37%), epichlorohydrin, concentrated ammonium hydroxide (NH_4OH, 30%), azure A dye, sodium hydroxide (NaOH), potassium bromide (KBr) and sodium chloride (NaCl) were all obtained from Sigma Aldrich (Missouri, USA). All the media (RPMI 1640 and Dulbecco's Modified Eagle Medium (DMEM)) and reagents (phosphate buffered saline (PBS), EDTA, fetal bovine serum (FBS) and antibiotics) for cell culture were obtained from Invitrogen (California, USA). Rat 9L-glioma cell line was obtained from the Brain Tumor Research Center (University of California San Francisco, USA). Deionized water (DI H_2O) for all reactions, solution preparation and sample purification was prepared from a Milli-Q A10 Biocel water purification system (Millipore, USA).

2.2 Synthesis of magnetic iron oxide nanoparticles (MNP)

2.2.1 Synthesis of DNPH—The hydroxyl groups of the coating starch on parent nanoparticles ("D") were cross-linked and aminated using epichlorohydrin and concentrated ammonium hydroxide (30%, w/v), respectively.[21,22] The aminated D particles ("DN") were then PEGylated ("DNP") with mPEG-NHS (20 kDa) using the simple N-hydroxysuccinimide (NHS) chemistry (Figure 1a). The PEGylated DN particles ("DNP") were desalted by dialysis using a 10-kDa molecular weight cut-off (MWCO) Slide-A-Lyzer dialysis cassette (Thermo Scientific, USA), purified and concentrated using a Dynal magnetic separator (Invitrogen, USA).

The simple EDC/NHS chemistry was employed for heparin conjugation of DNP nanoparticles. Briefly, 1 mL of heparin solution (20 mg/mL in 0.15 M PBS, pH 5.5) was mixed with EDC (20 mg), NHS (17 mg) and a catalytic amount of DMAP and incubated at 25 °C for 0.5 h. After heparin activation, 3 mL of DNP suspension (20 mg Fe/mL in 0.15 M PBS, pH 8.0) was added and the conjugation reaction was carried out by incubation at 25 °C for 2 h. This D-based, aminated, PEGylated and heparin conjugated MNP was then called as "DNPH" (Figure 1a). After conjugation, DNPH nanoparticles were also desalted via dialysis, purified and concentrated via magnetic separation.

2.2.2 Synthesis of HP—The above mentioned simple EDC/NHS chemistry was also used here for PEGylation of commercial fluidMAG-Heparin ("H") nanoparticles (Figure 1b). The carboxylate groups of the surface heparin of H were activated by EDC/NHS with a catalytic amount of DMAP first, and then conjugated to the amine group on the end of mPEG-NH_2 (Figure 1b). The PEGylated H nanoparticles were then called as "HP". This HP product was also desalted via dialysis, purified and concentrated via magnetic separation.

2.3 Characterization of MNP

2.3.1 Size distribution and zeta potential of MNP—The average intensity-weighted hydrodynamic size distribution and zeta potential of MNP suspensions were measured by dynamic light scattering (DLS) using a Nano ZS90 particle-sizer (Malvern, Worcestershire, UK). All the measurements were carried out in triplicate from dilute (~ 0.1 mg/mL) MNP suspensions in DI H_2O.

Size stability of each type of MNP against centrifugation was characterized using a multiple-centrifugation process. In detail, 1.0 mL of size-known MNP suspensions (2.4 mg Fe/mL, the same concentration of the suspensions used for *in vivo* studies) were centrifuged at 15,000 rounds per minute (r.p.m.) × 15 min for five times. Every time after centrifugation, the samples were re-suspended by pipetting, followed by a mild sonication (20 seconds, 10% amplitude) using a Sonifier operated at 10% (Branson, Danbury, CT) at 25 °C. The size distributions of the samples were monitored by DLS throughout the centrifugation process.

2.3.2 Measurements of amine, PEG and heparin content on MNP—A previously reported ninhydrin assay was used to quantify the amine content of DN by measuring the amine-initiated production of Ruhemann's Purple at 570 nm using a PowerWaveX340 spectrophotometer (Biotek, Vermont, USA).[23] To quantify the PEG chain density on MNP (DNP and HP), a barium iodide assay was used by measuring the absorbance of the complex of PEG and barium iodide at 535 nm.[24,25] In addition, azure A assay was chosen to quantify the heparin content of MNP (both DNPH and HP) by measuring the absorbance change at 620 nm based on the metachromatic shift of azure A from blue to red in the presence of heparin.[26]

All spectrophotometric analyses in this section were completed in triplicate.

2.3.3 Fourier transform infrared spectroscopy (FTIR), Transmission electronmicroscopy (TEM) and Superconducting Quantum Interference Device (SQUID) characterization of MNP—MNP suspensions were lyophilized prior to the collection of their infrared (IR) spectra using FTIR. MNP powder (2 ~ 3 mg) was mixed with spectroscopic grade KBr (~ 150 mg) and pressed into ~ 1-mm thick discs. A Spectrum BX FTIR spectrometer (Perkin Elmer, Massachusetts, USA) was used to record the IR spectra of the MNP. For TEM analysis, samples were prepared by applying dilute particle suspensions onto Lacey carbon film-coated copper grids followed by ambient drying. TEM images of MNP were conducted using a Philips CM-100 transmission electron microscope (Amsterdam, Netherlands) at an accelerated voltage of 60 kV. Magnetic susceptibility of MNP was assessed using a MPMS-XL SQUID magnetometer (Quantum Design, California, USA). Powder samples of MNP were suspended in an eicosane matrix, mounted in capsules and then analyzed at varying DC magnetic field (0-30000 Oe) at 300 K.

2.4 Protamine loading on DNPH

0-200 μL of protamine solution (500 μg/mL in DI H_2O) was added to 0.5 mL of DNPH suspension (2 mg Fe/mL in DI H_2O) and diluted to a total volume of 1.0 mL with DI H_2O. Protamine loading onto DNPH was carried out at 4 °C for 2 h with shaking. After

incubation, unbound protamine was removed by centrifugation at 15,000 r.p.m. for 15 min and subsequent wash with DI H_2O for three times. The protamine-loaded DNPH was then re-suspended in 1.0 mL of 1 mol/L NaCl and incubated at 25 °C for 30 min followed by 3 times of centrifugation at 15,000 r.p.m. × 20 min. All the supernatants were collected and brought to a total volume of 4 mL with 1 mol/L NaCl and the protamine amount was quantified by BCA protein assay. The protamine loading content (PLC) and protamine binding efficiency (PBE) were calculated according to the following equations (1-2):

$$\mathrm{PLC} = (\text{amount of loaded protamine}) / (\text{amount of Fe}) \quad (1)$$

$$\mathrm{PBE}\% = (\text{amount of loaded protamine}) / (\text{amount of feed protamine}) \times 100\% \quad (2)$$

The size distribution and zeta potential of protamine-loaded DNPH were also measured. And long term (up to six months) size stability and zeta potential change of DNPH and protamine-loaded DNPH in DI H_2O and PBS (0.15 mol/L, pH 7.2) were also monitored.

Protamine loading study for HP was not carried out in detail due to its instability with exposure to any amount of protamine.

2.5 *In vivo* evaluation of DNPH

All animal studies were carried out according to protocols reviewed and approved by the University of Michigan Committee on Use and Care of Animals (UCUCA).

2.5.1 Plasma pharmacokinetics (PK) of MNP—Male C57BL6 black mice (18-22 g, Harlan, Indiana, USA) were divided into three groups and separately administered with HP, DNP and DNPH through the lateral tail vein with a dose of 12 mg Fe/kg (body weight, BW). 100 μL of blood samples were collected by cardiac puncture at preset time points and centrifuged immediately at 5,000 r.p.m. × 5 min to obtain plasma. 30μL of plasma sample was added to an electron spin resonance (ESR) tube and the Fe content was quantified by ESR spectroscopy (detailed ESR procedures were described in Section 2.6.2).

A previously described one-compartment pharmacokinetic model[27] was applied to construct the plasma concentration-versus-time curves of the MNP samples and their PK profiles were acquired accordingly.

2.5.2 Biodistribution of MNP in mouse major organs—Male C57BL6 black mice were administered with different MNP samples (HP, DNP and DNPH) using the identical protocol described in Section 2.5.2. At 1 h and 48 h post-injection, mice were euthanized and their major organs (heart, liver, spleen, lung, and kidney) were collected. The MNP content in the organs were quantified by ESR spectroscopy.

2.5.3 Induction of 9L-glioma subcutaneous tumors—Left flank subcutaneous tumors of 9L-glioma were induced in male athymic nude mice (18-22 g, Harlan, Indianapolis, IN). In brief, 9L-glioma cells (Brain Tumor Research Center, University of California, San Francisco) were cultured to confluence in Dulbecco's modified Eagle's medium (DMEM) containing 10% heat inactivated FBS and 1% antibiotics (penicillin and streptomycin) in a humidified atmosphere containing 5% CO_2 at 37 °C.[18] Cells were harvested using trypsin-EDTA and re-suspended in serum-free fresh DMEM to a cell density of 10^8 cells/mL and the cell suspension (100 μL) was injected subcutaneously into the left flank of mice. When the tumor size reached 300-500 mm^3, the mice were used for magnetic targeting experiments.

2.5.4 Magnetic resonance imaging (MRI) and magnetic targeting—MRI experiments were carried out on a 30-cm horizontal-bore, 7T Direct Drive small animal imaging system (Varian, California, USA). Animals induced with flank tumors in Section 2.5.3 were anesthetized with isoflurane/air mixture (1.5/98.5 v/v) and imaged using a 3.5-cm-diameter quadrature RF head coil (m2m Imaging, OH, USA). Prior to the administration of MNP, the subcutaneous tumor was visualized *in vivo* using a high-resolution T2-weighted fast spin echo multi-slice (fsems) scan with the following parameters: Repetition time (TR), 4,000 ms; Echo time (TE), 60 ms; Slice thickness, 1 mm; Slice separation, 0 mm; Number of slices, 15; Field of view, 30 mm × 30 mm over 256 × 256 matrix.

For magnetic targeting, the magnetic setup consisted of a small D48-N52 cylindrical permanent ferro-magnet (6.4 mm-diameter × 12.7 mm-thickness, K&J Magnetics, USA) mounted on the pole of three DY0Y0-N52 cylindrical permanent ferro-magnets (51 mm diameter × 51 mm thickness) linked in tandem (Figure S1, supporting info). The magnetic field density at the pole face of the small magnet was about 320 mT measured using a Tesla-meter (MetroLab THM 7025 model, GMW Associates, California, USA). The tumor-bearing mouse was anesthetized and placed face-down on a platform with the tumor site positioning as close as possible to the pole of the small magnet. Each mouse was administered with MNP suspension at a dose of 12 mg Fe/kg via lateral tail vein and retained in magnetic field for 1 h.[27] The mice were imaged immediately after the magnetic targeting. Baseline T2-weighted images were acquired prior to MNP administration as well. The tumor-bearing mice injected with HP were also imaged before and after magnetic targeting for comparison.

2.5.5 Quantitative analysis of MNP content in excised tumor tissue—After MRI, flank tumors were excised from the mice and the MNP content wasmeasured using ESR spectroscopy. The percentage of injected MNP dose (I.D.%) accumulated in tumor tissue was calculated according to Equation (3):

$$\text{I.D.}\%/\text{g tissue} = [\text{MNP}]/\text{I.D.} \times \text{BW} \quad (3)$$

Here, [MNP] is Fe content in excised tumor tissue with a unit of (μg Fe/g tissue); BW was normalized as 20 g for each mouse, which means that the injected Fe amount for each MNP type was 240 μg Fe/mouse.

2.6 Quantitative analysis of MNP by the measurements of Iron (Fe) content

2.6.1 Fe content of MNP suspensions in DI H_2O—Fe content of the MNP in DI H_2O throughout this study was analyzed by inductively coupled plasma optical emission spectroscopy (ICP-OES) using an Optima DV 2000 spectrometer (Perkin Elmer, USA). Briefly, 10 μL of MNP sample was digested in 1 mL of concentrated HCl and diluted to a total volume of 10 mL with DI H_2O to a concentration of 1-10 mg Fe/L. Samples were analyzed in triplicate at 238.204 nm and calibrated using dilutions of iron standard (0-10 mg Fe/L) and yittrium internal standard (1 mg Fe/L).

2.6.2 Fe content of MNP in plasma samples and excised tissues—Quantitative analysis of MNP (Fe content) in all blood and excised tissue samples throughout this study was conducted using ESR spectroscopy. ESR spectra of the samples were acquired using an EMX ESR spectrometer (Bruker, Massachusetts, USA) with the key parameters set as: Temperature, -128 °C; Resonant frequency, 9.2 GHz; Microwave power, 20 mW.

The combination of receiver gain ($1 \times 10^3 \sim 1 \times 10^5$) and modulation amplitude (1G or 5G) varied according to the observed spectral intensity of different samples. WinEPR software (Bruker, Billerica, MA) was used to obtain the double integral (DI) values of the spectra.

2.7 Statistical analysis

All data were shown in this study as mean ± standard deviation (mean ± SD) unless otherwise noted. Statistical comparisons were made using the Student's *t*-test and $p < 0.05$ was considered significantly different.

3. Results

3.1 Synthesis, size and zeta potential characterization of MNP

Starch-coated MNP (D) have been widely utilized in both diagnostic and therapeutic applications in previous studies.[27-29] The coating starch is biocompatible and provides hydroxyl functional groups for additional conjugations. In order to further stabilize the coating starch and functionalize D for subsequent conjugation, D was crosslinked with epichlorohydrin and aminated with concentrated ammonia to form DN (Figure 1a). D and DN were characterized in detail for particle size distribution, surface charge density and amine content with the results shown in Table 1. After crosslinking, amination and PEGylation, the average hydrodynamic diameter of MNP increased slightly from 104.7 ± 1.7 nm (D) to 136.3 ± 5.5 (DN) and 165.1 ± 8.2 nm (DNP). And amination of D (−4.4 ± 0.5 mV) resulted in a huge and expectedpositive shift in zeta potential for DN (+38.9 ± 3.2 mV), indicating the successfulamination. And a shift of zeta potential toward neutral (from +38.9 ± 3.2 mV (DN) to+23.8 ± 2.7 mV (DNP)) was found after PEGylation, owing to the coverage of part ofthe MNP surface by the PEG neutral chains as well as the usage of amine groups forPEGylation. Both the increase of size and shifts of zeta potential of MNP indicatedthe satisfactory synthesis of DN and DNP. The amination of D was further confirmedand quantified using ninhydrin assay with the presence of dark Ruhemann's purple.The amine content of DN went as high as 278.1 ± 34.2 nmol/mg Fe. Based on theChemicell® product information of D (1.8×10^{12} particles/mg Fe, e.g., 9.95×10^{-3} pmol Fe/particle), there are about 9.27×10^4 amine groups/DN nanoparticle (1.5×10^{-4} pmol amine groups/particle). And the barium iodide assay further confirmed theconjugation of PEG to MNP with PEG content of 25.6 ± 5.8 μg/mg Fe and (usage ofNH_2)% of 0.46%, resulting in about 430 PEG molecules/DNP nanoparticle (7.0×10^{-7}pmol PEG/particle). Amine usage results also indicated that the vast majority ofamine groups (> 99%) on the surface of DNP remained available for subsequentheparin conjugation.

EDC/NHS chemistry was used for heparin conjugation onto DNP. Heparin has the highest negative charge density of any known biological molecule,[30,31] and thus, DNPH showed an expected negative shift of zeta potential after heparin conjugation from +23.8 ± 2.7 mV (DNP) to −2.1 ± 0.7 m V. However, due to the much longer chain of PEG than that of heparin, average hydrodynamic diameter of MNP remained almost the same (DNP of 165.1 ± 8.2 nm vs. DNPH of 168.8 ± 9.9 nm) after heparin conjugation. The azure A assay data showed a conjugation of 35.4 ± 4.3 μg heparin/mg Fe (1.3×10^{-6} pmol heparin/particle). The negative shift of zeta potential and the heparin content results shown here both confirmed the correct preparation of DNPH.

The EDC/NHS chemistry was also used for the PEGylation of commercial heparin-coated MNP (H) (Figure 1b). After PEGylation, size distribution of HP increased from 105.1 ± 2.2 nm (H) to 145.1 ± 7.9 nm and zeta potential of HP increased from −38.8 ± 3.3 mV (H) to −23.1 ± 3.7 mV. The HP carried a PEG content of 24.6 ± 4.4 μg/mg Fe (about 413 PEG molecules/HP nanoparticle) and a heparin content of 102.6 ± 3.5 μg heparin/mg Fe (3.4 ×

10^{-6} pmol heparin/particle). Compared to DNPH, HP had similar PEG content and about 3-fold higher heparin content.

In vitro size stability of MNP against centrifugation was characterized in detail.[31] As shown in Figure 2, both DNP and DNPH showed barely no difference between their size distributions and only slightly increases of hydrodynamic diameters were observed, indicating the great physical stability of DNP and DNPH against multiple cycles of centrifugation. Furthermore, DNP and DNPH were readily re-suspended in DI H_2O after the fifth centrifugation using mild sonication (10% amplitude, 20 seconds) with almost no size increases compared to those before centrifugation. However, in case of HP, its hydrodynamic diameter doubled (from 145.1 ± 7.9 nm to 290.4 ± 23.7 nm) after four times of centrifugation and even micro-particles (up to 10 microns) were observed after the fifth centrifugation (data not shown here). And size stability studies for H, D and DN against centrifugation were not performed in detail, as they could not be thoroughly re-suspended in DI H_2O with/without sonication even after the first centrifugation.

This good stability profile of DNPH allows rapid purification of the particles by centrifugation, instead of utilizing the more time-consuming purification using dialysis and magnetic separation.

3.2 FTIR, TEM and SQUID characterization of MNP

FTIR spectra (Figure 3a, b) further confirmed the correct synthesis of DNP, DNPH and HP. Evolution of the peak at ~1100 cm^{-1} in DNP and HP spectrum is the specific absorption of "C-O-C" ether bond stretching vibrations from PEG moieties,[32] indicating the successful PEGylation of DN and H to DNP and HP, respectively. And the absorption peak at ~1700 cm^{-1} in DNPH spectrum comes from the "–C=O" stretching vibrations of carboxyl group from heparin moieties,[33] proving the heparin conjugation with DNP.

The typical morphology of MNP was exhibited from the TEM images (Figure 4). As seen, all the MNP samples (D, DN, DNP, DNPH, H and HP) were observed as well-dispersed nanoparticles with approximately 100-200 nm size and irregular shape (larger coated cores comprised of multiple smaller Fe_3O_4 domains), indicating that MNP maintained their structure throughout the synthesis steps.

Magnetization properties of all MNP types were measured by SQUID to assess their susceptibility for magnetic targeting *in vivo*. As shown in Figure 5, the magnetization curves confirmed superparamagnetic characteristics of each MNP type (neither hysteresis nor magnetic remanence was observed). The magnetic properties of DNP (64.17 emu/g Fe), DNPH (56.99 emu/g Fe) and HP (59.84 emu/g Fe) showed slightly lower than those of their precursors of D (70.25 emu/g Fe) and H (67.38 emu/g Fe). The final candidates of DNPH and HP both kept more than 80% of the saturation magnetization of their respective parent MNP, indicating their plausibility for live animal magnetic targeting.

3.3 Protamine loading

As shown in Figure 6, protamine loading content (PLC) was significantly elevated ($p < 0.01$) from 4.9 ± 0.3 μg/mg Fe to 22.9 ± 4.7 μg/mg Fe by increasing feed protamine amount from 5 μg/mg Fe to 100 μg/mg Fe. When the feed protamine amount was raised from 60 μg/mg Fe (with PLC of 21.3 ± 3.6 μg/mg Fe) to 120 μg/mg Fe (with PLC of 22.9 ± 4.7 μg/mg Fe), there was only 1.6 μg/mg Fe increase in the PLC, suggesting saturation occurred for binding of protamine to DNPH. According to Figure 6, protamine binding efficiency (PBE) to DNPH decreased accordingly with the increase of feed protamine amount. The PBE was 98% when the feed protamine was 5 μg/mg Fe. However, only 19.1 % of feed protamine could bind to DNPH when feed protamine increased to 120 μg/mg Fe.

Compared to DNPH, the protamine-loaded nanoparticles (with maximum protamine loading) showed negligible change in size distribution and positive shift in zeta potential (+42.1 ± 6.6 mV). DNPH, with or without protamine loading, even showed negligible changes in size distribution and zeta potential during a period of six months in DI H_2O or PBS at 4 °C. The average hydrodynamic diameter and zeta potential of protamine loaded DNPH varied from (167.6 ± 8.7 nm and +42.1 ± 6.6 m V, freshly synthesized) to (169.4 ± 10.7 nm and +41.3 ± 7.2 mV, 1 month post-synthesis), (172.4 ± 9.8 nm and +43.4 ± 5.9 mV, 3 months post-synthesis) and (170.7 ± 7.4 nm and +40.8 ± 8.3 m V, 6 months post-synthesis).

3.4 PK profiles of MNP *in vivo*

To measure the *in vivo* stability of MNP (DNP, DNPH and HP), their PK profiles were investigated in C57BL6 mice. The plasma concentration-versus-time profiles are shown in Figure 7 and the estimated PK parameters are summarized in Table 2. All the tested MNP samples fit a one-compartment model (r^2 of 0.99). DNPH ($T_{1/2}$ = 9.37 h, CL = 8.58 mL/h/kg) showed markedly longer residence in the blood circulation than that of HP ($T_{1/2}$ = 0.15 h, CL = 885.08 mL/h/kg). On the other hand, the V_d for HP (191.08 mL/kg) was significantly higher ($p < 0.05$) than that of DNPH (115.94 mL/kg) indicating more extensive tissue distribution of HP (most likely in the liver and spleen, and thus, out of circulation). $AUC_{0-\infty}$ value for DNPH (1490 μg Fe·h/mL) was 106-fold higher than that of HP (14 μg Fe·h/mL). Without surface heparin, and thus, with least plasma protein binding,[34,35] DNP showed the longest blood circulation time with a half-life of 12.60 h and $AUC_{0-\infty}$ of 1957 μg Fe·h/mL.

3.5 Biodistribution of MNP in major mouse organs

The biodistribution profiles of MNP (DNP, DNPH and HP) at 1 hr and 48 hr post-injection were examined in C57BL6 mice. Based on the results of the PK study, 1 h and 48 h are the time spans needed for almost complete clearance of HP and D-based MNP (DNP or DNPH) from the blood circulation. As shown in Figure 8, similar MNP accumulation profiles were observed in heart (< 3 μg/g tissue), lung (about 10 μg/g tissue) and kidney (about 7 μg/g tissue). However, HP showed different accumulation profiles in the major elimination organs (liver and spleen), compared with those of DNP and DNPH. HP accumulated with high extents in both liver (148.33 ± 28.29 μg/g tissue @ 1 h post-injection and 84.76 ± 15.42 μg/g tissue @ 48 h post-injection) and spleen (196.65 ± 19.75 μg/g tissue @ 1 h post-injection and 139.32 ± 19.31 μg/g tissue @ 48 h post-injection). Notably, HP concentrations in both the liver and spleen at 48 h post-injection significantly decreased ($p < 0.05$) by 43% and 30%, respectively, from those at 1 h post-injection, presumably due to the degradation of the particles in the organs. In sharp contrast to the biodistribution profiles of H P, both DNP and DNPH displayed significantly much lower accumulations in the liver, but higher level in the spleen. Moreover, the concentrations of both DNP and DNPH in the liver at 48 h post-injection (DNP of 53.26 ± 12.96 μg/g tissue, DNPH of 60.44 ± 16.29 μg/g tissue) were slightly higher than those at 1 h post-injection (DNP of 43.64 ± 9.36 μg/g tissue, DNPH of 45.82 ± 11.35 μg/g tissue), possibly explained by their long circulating properties. Similar results were observed in spleen that MNP extents in spleen at 1 h post-injection were 117.89 ± 14.83 μg/g tissue (DNP) and 108.28 ± 17.87 μg/g tissue (DNPH), which increased markedly ($p < 0.01$) to 775.89 ± 87.67 μg/g tissue and 744.37 ± 98.95 μg/g tissue, respectively. Measured spleen MNP contents of DNP and DNPH are 6.6-fold and 6.9-fold higher, respectively, at 48 h post-injection than those at 1 h post-injection (Figure 8).

3.6 MRI monitoring of magnetic targeting of MNP in a mouse 9L-glioma model

MRI was used to monitor the magnetic tumor targeting of DNPH and HP. MNP are well-known as favorable enhancers of T2/T2* proton relaxation and thus could be identified as

hypointense (negative contrast) regions on T2-weighted fsems MRI scans.[12] The MNP induced signal decrease in T2-weighted MRI images presented valued information about the delivery of nanoparticles to the flank tumor lesion. Representative MRI images of mice administered with MNP with/without magnetic targeting were shown in Figure 9. In baselineT2-weighted fsems scan images (pre-targeting or pre-injection), the region of tumor (in broken circle) is clearly visible as a hyperintense region located subcutaneously on the left flank. The difference in the hypointensity of the tumor lesion of HP obtained by fsems scans at pre-/post-administration was negligible when magnetic targeting was not applied and only slightly enhanced hypointensity in the tumor region was observed when magnetic targeting was applied. This low magnetic tumor targeting could be explained by the poor plasma behavior of HP (short plasma half-life, low $AUC_{0-\infty}$ value). In a sharp contrast, after magnetic targeting, mice administered with long-circulating MNP (DNP or DNPH) displayed markedly enhanced hypointensity in the tumor regions. Notably, slight increase in the hypointensity of the tumor region was also observed even when the DNP or DNPH was administered without magnetic targeting, which could be explained by the enhanced permeation and residence (EPR) effect.

3.7 Quantitative analysis of Fe content in excised tumor tissue

The magnetic capture of DNPH, DNP or HP in tumor lesion was quantitatively analyzed with the same dose of 12 mg Fe/kg via intravenous administration for each MNP type. Quantitative MNP analysis in flank tumor lesions was presented in Figure 10. Because of the short plasma half-life of HP (about 9 min), the accumulation of HP in tumor lesion with or without magnetic targeting were 0.32 ± 0.21 μg Fe/g tissue (0.13% I.D./g tissue) and 4.27 ± 0.65 μg Fe/g tissue (1.78% I.D./g tissue), respectively. HP exposed tumors possessed statistically lower ($p < 0.01$) MNP concentrations compared to those exposed to either DNP or DNPH. And tumor Fe contents were about 5-fold higher after magnetic targeting for DNP (30.28 ± 4.76μg Fe/g tissue, 12.62% I.D./g tissue) and DNPH (31.36 ± 5.12 μg Fe/g tissue, 13.07% I.D./g tissue) than their non-targeted counterparts of DNP (6.32 ± 2.05 μg Fe/g tissue, 2.63% I.D./g tissue) and DNPH (6.08 ± 1.33 μg Fe/g tissue, 2.53% I.D./g tissue). DNP and DNPH showed slightly but not statistically different average tumor Fe concentrations for both non-targeted and targeted mice. Combining the long-circulating properties of MNP, EPR effect in tumor lesions and magnetic targeting, the tumor MNP concentration of DNP or DNPH was about 100-fold (non-targeted) and 7.5-fold (targeted) higher than those of HP, respectively. Encouragingly, this long-circulating DNPH even showed about 1.5-fold higher MNP accumulation in the non-targeted tumor than that of HP in the targeted tumor.

4. Discussion

In this study, a promising MNP platform was successfully synthesized using the simple EDC/NHS chemistry. All the results enabled this DNPH platform to be used as a promising candidate for magnetic tumor targeting and therapy: (1) it possessed a superparamagnetic core with an appropriate size (about 100 nm) suitable for magnetic capture and retention; (2) it showed long-circulating behaviors *in vivo* with a plasma half-life of 9.37 h, guaranteeing a sustained circulation delivery of DNPH to the targeted tumor tissue; (3) heparin-modification enabled DNPH to load therapeutic protein drugs (by simple charge interaction) for targeted tumor therapy. In general, MNP with larger magnetic cores are more sensitive to magnetic field, and thus, favor magnetic capture of MNP with higher concentrations in targeted tumors. However, larger size can increase the visibility of MNP to the RES (resulting in faster clearance) and decrease the surface area-to-volume ratio (resulting in lower drug loading content).[27] Considering these advantages and disadvantages, D with magnetic core size of about 100 nm was chosen, aminated, PEGylated and heparin functionalized for long-circulation, high drug loading content and superior magnetic

targeting *in vivo*. Moreover, some researches showed that accumulation of MNP in tumor lesions could be size-dependent, larger MNP (> 40nm) are desirable for higher tumor localization due to a longer retention time of larger particles *via* EPR effect.[36]

Protamine was chosen as a model cationic protein to prove the plausibility of the strong binding capability of DNPH for cationic cargoes, especially CPP-linked therapeutic proteins. DNPH kept stable with any tested protamine concentration (0 ~ 120 μg/mL) and showed a maximum PLC of 22.9 ± 4.7 μg/mg Fe. The intense charge interaction between heparin (on DNPH surface) and protamine could only be broken down when exposed to a high concentration (≥ 1 mol/L) of NaCl solution. Almost no protamine was detached from DNPH after a 1-h incubation of DNPH/heparin complex in 0.5 mol/L NaCl solution (data not shown). The strong binding of DNPH for protamine showed a promising future for this platform to be used as a carrier for CPP-modified proteins. Commercially available H with similar size of magnetic core was chosen and PEGylated for comparison. HP has about 3-fold more surface heparin than that of DNPH. However, this higher content of surface heparin didn't help HP for better stability (*in vitro* or *in vivo*) or protamine loading profiles. In fact, HP, with similar PEGylation (413 PEG molecules/particle) to that of DNPH (430 PEG molecules/particle), was very unstable and precipitated at once with exposure to any amount of protamine. The high density of heparin on HP enables intense charge interactions of HP with cationic cargoes, which could result in an electrostatic interaction-induced cross-linking. As a result, much larger particles were produced and huge precipitation happened.

For *in vivo* studies, HP showed a very short plasma circulation time with only about 8.5% I.D. left in the blood circulation at 30 min post-administration. Too much heparin on the nanoparticle surface caused severe binding of blood proteins and accelerated the opsonization of MNP, resulting in their faster blood clearance by tissue macrophages of the reticuloendothelial system (RES).[34,35] As a result, almost all the injected HP particles were trapped by liver (148.33 ± 28.29 μg/g tissue) and spleen (196.65 ± 19.75 μg/g tissue) at 1 h post-injection. Compared to H P, DNPH or DNP showed a totally different biodistribution pattern, especially the MNP accumulations in liver and spleen. Both DNP and DNPH showed long-circulating properties and relatively low accumulations in liver but high accumulations in spleen due to the modification of their surface properties with dysopsonic PEG polymer. The hydrophilic and flexible PEG segments can prevent the opsonin-nanoparticle interaction, which is the first step of the recognition by the immune system. The extension of nanoparticles' blood circulation time and reduced opsonin-nanoparticle interaction enable nanoparticles to reach other immune organs than liver, such as spleen. Furthermore, PEGylation of nanoparticles can result in a reduced uptake by the Kupffer cells (main macrophages in liver) and an increased uptake by splenic macrophages. Although the exact mechanism of this phenomenon was unclear, this general trend has been observed for several decades for many kinds of nanoparticle types.[37-39] As a result, accumulations of DNP and DNPH in spleen were 2.7-fold and 2.4-fold (at 1 h post-injection) and 14.5-fold and 12.4-fold (at 48 h post-injection) higher than those in liver, respectively. The different PK and biodistribution profiles between HP and DNPH (or DNP) also indicated the limited protection of PEG chain for MNP. Even with similar PEG density on particle surface, DNP or DNPH, without or with much less coating heparin, showed 84-fold or 62-fold longer plasma half-life and 140-fold or 106-fold better MNP exposure (AUC) than those of H P. Although heparin is a key part of this MNP-based drug delivery system, too much coating heparin will cause a lot of adverse effects. DNPH with reasonable heparin content showed the best potential in CPP-linked protein loading and tumor therapy in the future.

DNPH showed very similar PK and biodistribution profiles to those of heparin-free DNP. Even so, DNPH holds a brighter future than that of DNP based on its capability or potential

for cationic drug loading and selective delivery. This heparin-modified DNPH platform showed a simple, stable, efficient and reversible loading for cationic protamine. However, DNP, without coating heparin or any other binding/attachment moieties, could not be directly employed for drug loading/attachment and further tumor therapy.

The elimination of MNP from liver and spleen was also coarsely measured in this study. For long-circulating DNP and DNPH, it's difficult to measure their precise elimination rate *in vivo* due to the coexistence of MNP accumulation and elimination in liver and spleen. However, the coarse elimination degree of HP could be acquired by calculating the decrease of MNP concentrations in liver and spleen from 1 h to 48 h post-injection. Up to 43% of HP in liver and 30% of HP in spleen were cleared out from 1 h to 48 h post-injection, proving the satisfactory elimination of MNP from immune organs.

All the encouraging *in vitro/in vivo* results inspired us to move further. DNPH system was tested for magnetic targeting in a 9L-glioma tumor bearing mouse model monitored by MRI. Exact MNP content in excised tumor tissue was also measured by ESR analysis. MRI scans supplied very intuitionistic images of MNP accumulation in tumor lesions. However, it's difficult to tell the difference between images when MNP contents in tumor tissue were close to each other or very low (less than 10 μg/g tissue). Almost no difference could be observed between images of D-injected mice with/without magnetic targeting, even the Fe content in targeted tumor tissue (4.27 ± 0.65 μg/g tissue) was 14-fold higher than that in non-targeted tumor tissue (0.32 ± 0.21 μg/g tissue). For ESR analysis, it takes longer time and more steps to get the magnetic targeting results. However, it gives more precise and reliable results of MNP contents in excised tumor tissue. Due to the inhomogeneity of tumor tissue as well as magnetic strength, multi-samples should be prepared from the same excised tumor for ESR analysis, which is crucial to get reliable average tumor MNP concentrations.

5. Conclusion

DNPH was successfully synthesized by cross-linking, amination, PEGylation and heparin conjugation of the commercially acquired starch-coated MNP (D). This multifunctional MNP platform showed almost perfect resistance against high speed centrifugation (15,000 r.p.m.), long-circulating PK with a plasma half-life of 9.37 h and expected protamine loading performance with a PLC of 22.9 μg/mg Fe. The binding of DNPH for cationic protamine is simple, efficient, stable and reversible. MR images and ESR quantitative analysis both confirmed that the applied magneitc field (320 mT) can selectively and effectively deliver this long-circulating DNPH to tumor tissue with MNP accumulation of as high as 31.36 μg Fe/g tissue (13.07% I.D./g tissue) at 1 h post-targeting. These promising results encourage us to load a therapeutic protein to DNPH for efficacy study. This work is on-going currently in our lab in a rat 9L-glioma brain tumor model.

Supplementary Material

Refer to Web version on PubMed Central for supplementary material.

Acknowledgments

This work was supported in part by the National Institutes of Health (NIH) R01 Grants CA114612 and NS066945, and a Hartwell Foundation Biomedical Research Award. This work was also partially sponsored by Grant R31-2008-000-10103-01 from the World Class University (WCU) project of South Korea. Victor C. Yang is currently a participating faculty member in the Department of Molecular Medicine and Biopharmaceutical Sciences, Seoul National University, South Korea. In, addition, the project was partially sponsored by the National Basic Research Program of China (973 Program) 2013CB932502.

References

1. Siegel R, Naishadham D, Jemal A. Cancer statistics 2013. CA-Cancer J Clin. 2013; 63:11–30. [PubMed: 23335087]
2. Va n Meir EG, Hadjipanayis CG, Norden AD, Shu HK, Wen PY, Olson JJ. Exciting new advances in neuro-oncology the avenue to a cure for malignant glioma. CA-Cancer J Clin. 2010; 60:166–193. [PubMed: 20445000]
3. Kohler BA, Ward E, McCarthy BJ, Schymura MJ, Ries LAG, Eheman C, Jemal A, Anderson RN, Ajani UA, Edwards BK. Annual report to the nation on the status of cancer, 1975–2007, featuring tumors of the brain and other nervous systemr. J Natl Cancer Inst. 2011; 103:714–736. [PubMed: 21454908]
4. Zhou XK, Qiu J, Wang Z, Huang NY, Li XL, Li Q, Zhang YB, Zhao CJ, Luo C, Zhang NN, Teng X, Chen ZW, Liu X, Yu XL, Wu WL, Wei YQ, Li L. *In vitro* and *in vivo* anti-tumor activities of anti-EGFR single-chain variable fragment fused with recombinant gelonin toxin. J Cancer Res Clin Oncol. 2012; 138:1081–1090. [PubMed: 22392077]
5. Wang JT, Giuntini F, Eggleston IM, Bown SG, MacRobert AJ. Photochemical internalisation of a macromolecular protein toxin using a cell penetrating peptide-photosensitiser conjugate. J Control Release. 2012; 157:305–313. [PubMed: 21889554]
6. Cao Y, Marks JW, Liu Z, Cheung LH, Hittelman WN, Rosenblum MG. Design optimization and characterization of Her2/neu-targeted immunotoxins: comparative in vitro and *in vivo* efficacy studies. Oncogene. 2013; 32:1–11.
7. Liu Z, Winters M, Holodniy M, Dai HJ. siRNA delivery into human T cells and primary cells with carbon-nanotube transporters. Angew Chem. 2007; 46:2023–2027. [PubMed: 17290476]
8. Lee JH, Lee K, Moon SH, Lee YH, Park TG, Cheon J. All-in-One target-cell-specific magnetic nanoparticles for simultaneous molecular imaging and siRNA delivery. Angew Chem. 2009; 121:4238–4243.
9. Valadi H, Ekstrom K, Bossios A, Sjostrand M, Lee JJ, Lotvall JO. Exosome-mediated transfer of mRNAs and microRNAs is a novel mechanism of genetic exchange between cells. Nat Cell Biol. 2007; 9:654–670. [PubMed: 17486113]
10. Park YJ, Chang LC, Liang JF, Moon C, Chung CP, Yang VC. Nontoxic membrane translocation peptide from protamine, low molecular weight protamine (LMWP), for enhanced intracellular protein delivery: *in vitro* and *in vivo* study. Faseb J. 2005:1555–1557. [PubMed: 16033808]
11. Kwon YM, Li YT, Naik S, Liang JF, Huang YZ, Park YJ, Yang VC. The ATTEMPTS delivery systems for macromolecular drugs. Expert Opin Drug Del. 2008; 5:1255–1266.
12. Reddy LH, Arias JL, Nicolas J, Couvreur P. Magnetic nanoparticles: design and characterization, toxicity and biocompatibility, pharmaceutical and biomedical applications. Chem Rev. 2012; 112:5818–5878. [PubMed: 23043508]
13. Xie J, Liu G, Eden HS, Ai H, Chen XY. Surface-engineered magnetic nanoparticle platforms for cancer imaging and therapy. Acc Chem Res. 2011; 44:883–892. [PubMed: 21548618]
14. Yoo DW, Lee JH, Shin TH, Cheon JW. Theranostic magnetic nanoparticles. Acc Chem Res. 2011; 44:863–874. [PubMed: 21823593]
15. Colombo M, Carregal-Momero S, Casula MF, Gutierrez L, Morales MP, Bohm IB, Heverhagen JT, Prosperi D, Parak WJ. Biological applications of magnetic nanoparticles. Chem Soc Rev. 2012; 41:4306–4334. [PubMed: 22481569]
16. Lee SM, Song Y, Hong BJ, MacRenaris KW, Mastarone DJ, O'Halloran TV, Meade TJ, Nguyen ST. Modular polymer-caged nanobins as a theranostic platform with enhanced magnetic resonance relaxivity and pH-responsive drug release. Angew Chem. 2010; 122:10156–10160.
17. Sanson C, Diou O, Thevenot J, Ibarboure E, Soum A, Brulet A, Miraux S, Thiaudiere E, Tan S, Brisson A, Dupuis V, Sandre O, Lecommandoux S. Doxorubicin loaded magnetic polymersomes: theranostic nanocarriers for MR imaging and magneto-chemotherapy. ACS Nano. 2011; 5:1122–1140. [PubMed: 21218795]
18. Chertok B, David AE, Yang VC. Magnetically-enabled and MR-monitored selective brain tumor protein delivery in rats via magnetic nanocarriers. Biomaterials. 2011; 32:6245–6253. [PubMed: 21632104]

19. Sun CR, Du K, Fang C, Bhattarai N, Veiseh O, Kievit F. PEG-mediated synthesis of highly dispersive multifunctional superparamagnetic nanoparticles: their physicochemical properties and function *in vivo*. ACS Nano. 2010; 4:2402–2410. [PubMed: 20232826]
20. Torchilin V. Tumor delivery of macromolecular drugs based on the EPR effect. Adv Drug Deliver Rev. 2011; 63:131–135.
21. Pittet MJ, Swirski FK, Reynolds F, Josephson L, Weissleder R. Labeling of immune cells for *in vivo* imaging using magnetofluorescent nanoparticles. Nat Protoc. 2006; 1:73–79. [PubMed: 17406214]
22. Simkovic I, Laszlo JA, Thompson AR. Preparation of a weakly basic ion exchanger by crosslinking starch with epichlorohydrin in the presence of NHAOH. Carbohyd Polym. 1996; 30:25–30.
23. Prochazkova S, Varum KM, Østgaard K. Quantitative determination of chitosans by ninhydrin. Carbohydr Polym. 1999; 38:115–122.
24. Skoog B. Determination of polyethylene glycols 4000 and 6000 in plasma protein preparations. Vox Sang. 1979; 37:345–349. [PubMed: 44395]
25. Kurfurst MM. Detection and molecular weight determination of polyethylene glycol-modified hirudin by staining after sodium dodecyl sulfate-polyacrylamide gel electrophoresis. Anal Chem. 1992; 200:244–248.
26. Ma SC, Fu B, Meyerhoff ME, Yang VC. Electrochemical sensor for heparin: further characterization and bioanalytical applications. Anal Chem. 1993; 65:2078–2084. [PubMed: 8372971]
27. Cole AJ, David AE, Wang JX, Galban CJ, Hill HL, Yang VC. Magnetic brain tumor targeting and biodistribution of long-circulating PEG-modified, cross-linked starch-coated iron oxide nanoparticles. Biomaterials. 2011:2183–2193. [PubMed: 21176955]
28. Richter H, Kettering M, Wiekhorst F, Steinhoff U, Hilger I, Trahms L. Magnetorelaxometry for localization and quantification of magnetic nanoparticles for thermal ablation studies. Phys Med Biol. 2010; 55:624–634.
29. Chertok B, David AE, Yang VC. Polyethyleneimine-modified iron oxide nanoparticles for brain tumor drug delivery using magnetic targeting and intra-carotid administration. Biomaterials. 2010; 31:6317–6324. [PubMed: 20494439]
30. Gott VL, Whiffen JD, Dutton RC. Heparin bonding on colloidal graphite surfaces. Science. 1963; 142:1297–1298. [PubMed: 14074839]
31. Cheng JJ, Teply BA, Sherifi I, Sung J, Luther G, Gu FX, Levy-Nissenbaum E, Radovic-Moreno AF, Langer R, Farokhzad OC. Formulation of functionalized PLGA–PEG nanoparticles for *in vivo* targeted drug delivery. Biomaterials. 2007; 28:869–876. [PubMed: 17055572]
32. Xie J, Xu C, Kohler N, Hou Y, Sun S. Controlled PEGylation of monodisperse Fe3O4 nanoparticles for reduced non-specific uptake by macrophage cells. Adv Mater. 2007; 19:3163–3166.
33. Singh S, Wu BM, Dunn JCY. The enhancement of VEGF-mediated angiogenesis by polycaprolactone scaffolds with surface cross-linked heparin. Biomaterials. 2011; 32:2059–2069. [PubMed: 21147501]
34. Young E, Wells P, Holloway S, Weitz J, Hirsh J. Ex-vivo and in-vitro evidence that low molecular weight heparins exhibit less binding to plasma proteins than unfractionated heparin. Thromb Haemost. 1994; 71:300–304. [PubMed: 8029793]
35. Young E, Cosmi B, Weitz J, Hirsh J. Comparison of the non-specific binding of unfractionated heparin and low molecular weight heparin (enoxaparin) to plasma proteins. Thromb Haemost. 1993; 70:625–630. [PubMed: 8115988]
36. Larsen EKU, Nielsen T, Wittenborn T, Birkedal H, Vorup-Jensen T, Jakobsen MH, Østergaard L, Horsman MR, Besenbacher F, Howard KA, Kjems J. Size-dependent accumulation of PEGylated silane-coated magnetic iron oxide nanoparticles in murine tumors. ACS Nano. 2009; 3:1947–1951. [PubMed: 19572620]
37. Nel AE, Madler L, Velegol D, Xia T, Hoek EMV, Somasundaran P, Klaessig F, Castranova V, Thompson M. Understanding biophysicochemical interactions at the nano-bio interface. Nat Mater. 2009; 8:543–557. [PubMed: 19525947]

38. Lankveld DPK, Rayavarapu RG, Krystek P, Oomen AG, Verharen HW, Leeuwen TG, Jong WHD, Manohar S. Blood clearance and tissue distribution of PEGylated and non-PEGylated gold nanorods after intravenous administration in rats. Nanomedicine. 2011; 6:339–349. [PubMed: 21385136]

39. Peracchia MT, Fattal E, Desmaele D, Besnard M, Noel JP, Gomis JM, Appel M, d'Angelo J, Couvreur P. Stealth PEGylated polycyanoacrylate nanoparticles for intravenous administration and splenic targeting. J Control Release. 1999; 60:121–128. [PubMed: 10370176]

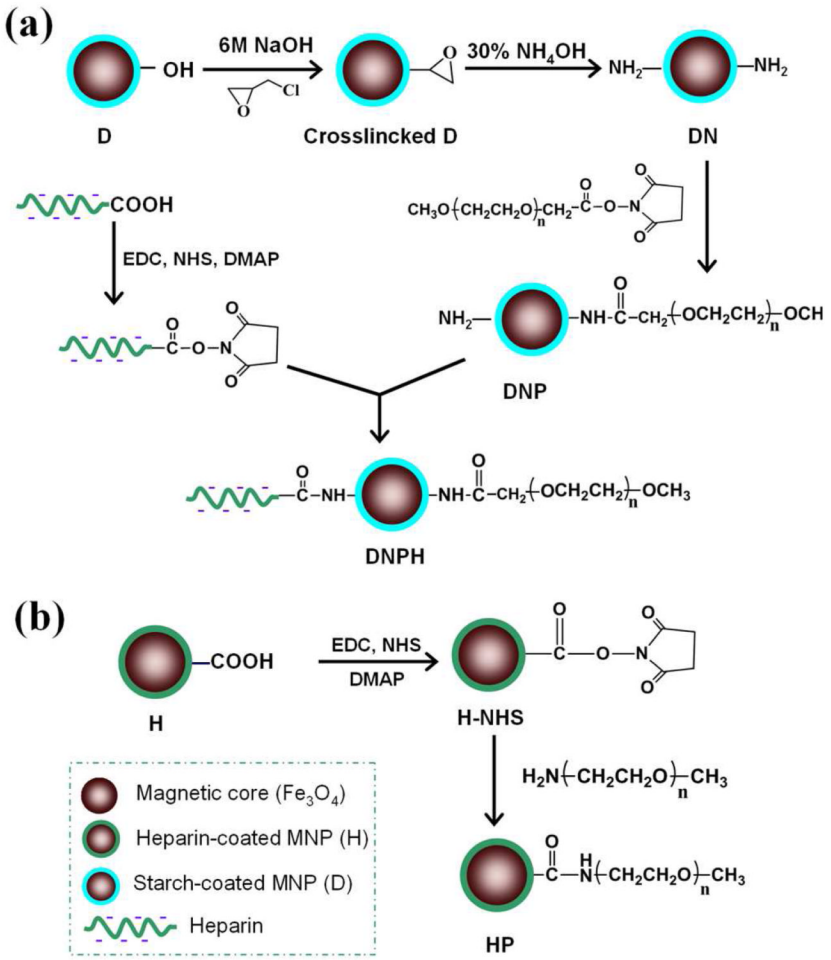

Figure 1.

(a) Synthesis strategy of DNPH by crosslinking, amination, PEGylation and heparin modification of commercial starch-coated MNP (D); (b) Synthesis strategy of HP by PEGylation of heparin-coated MNP (H).

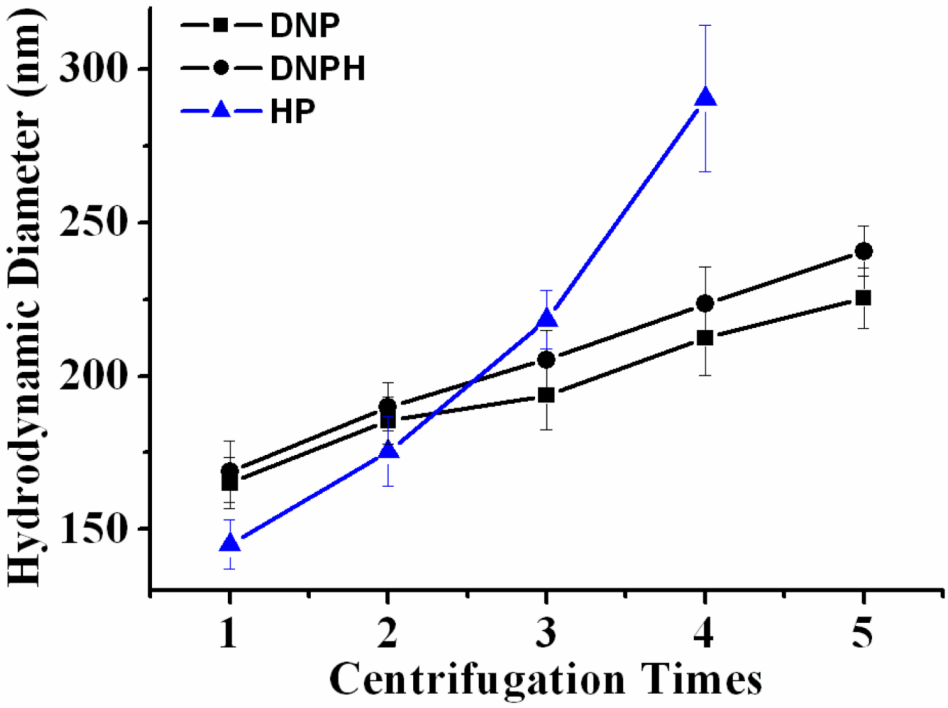

Figure 2.
Size stability of DNP, DNPH and HP against centrifugations at 15,000 r.p.m. @ 15 min × 5. The samples were re-suspended in DI H_2O by pipetting with/without 20 seconds of sonication after the centrifugation.

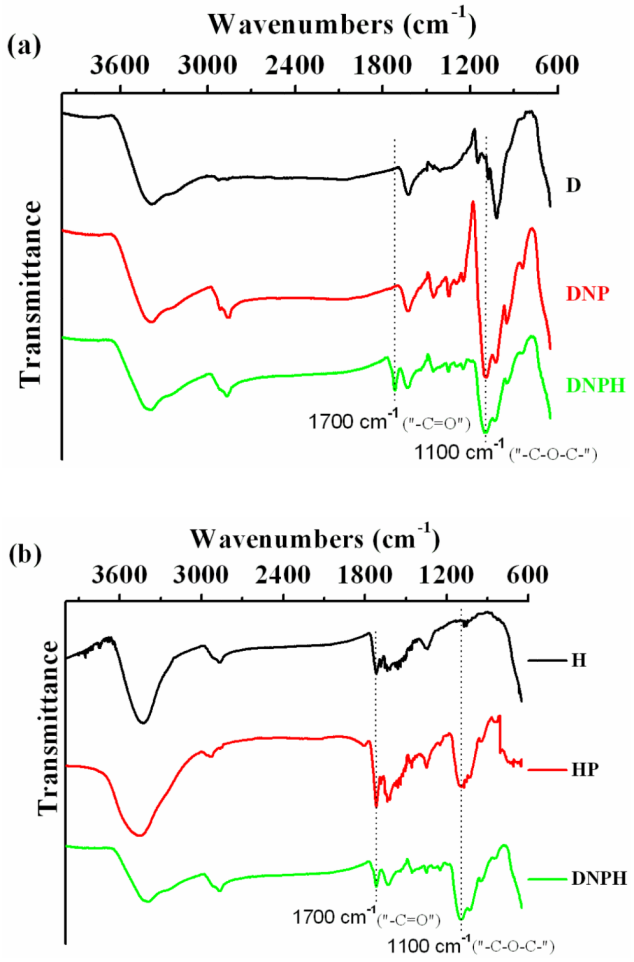

Figure 3.
FTIR spectra of lyophilized MNP powders: (a) D, DNP and DNPH; (b) H, HP and DNPH.

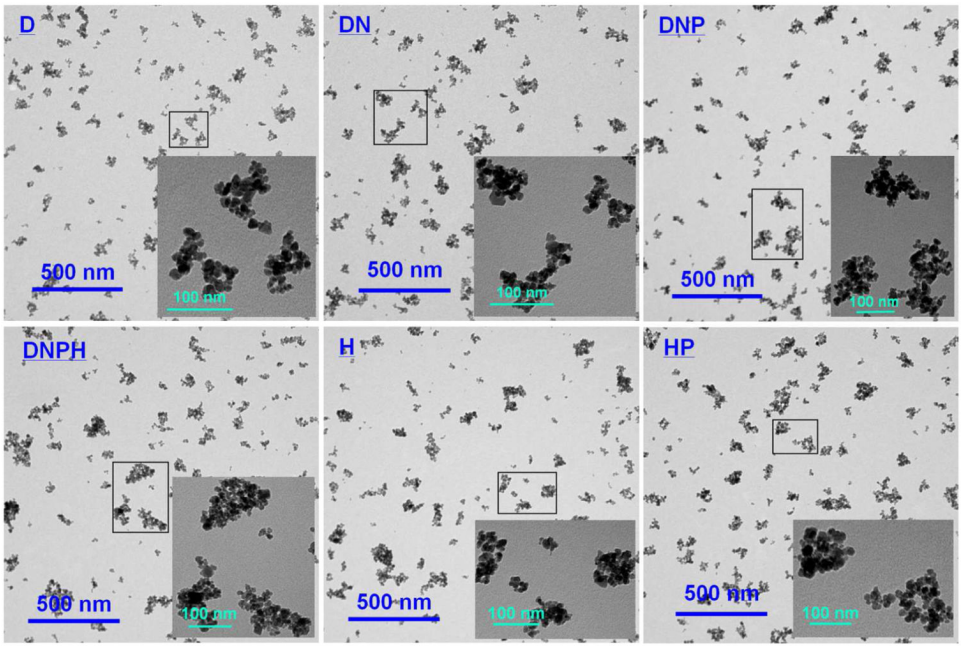

Figure 4.
TEM images of all MNP types (D, DN, DNP, DNPH, H and HP). Inset images: magnification of the representative nanoparticles of each MNP type.

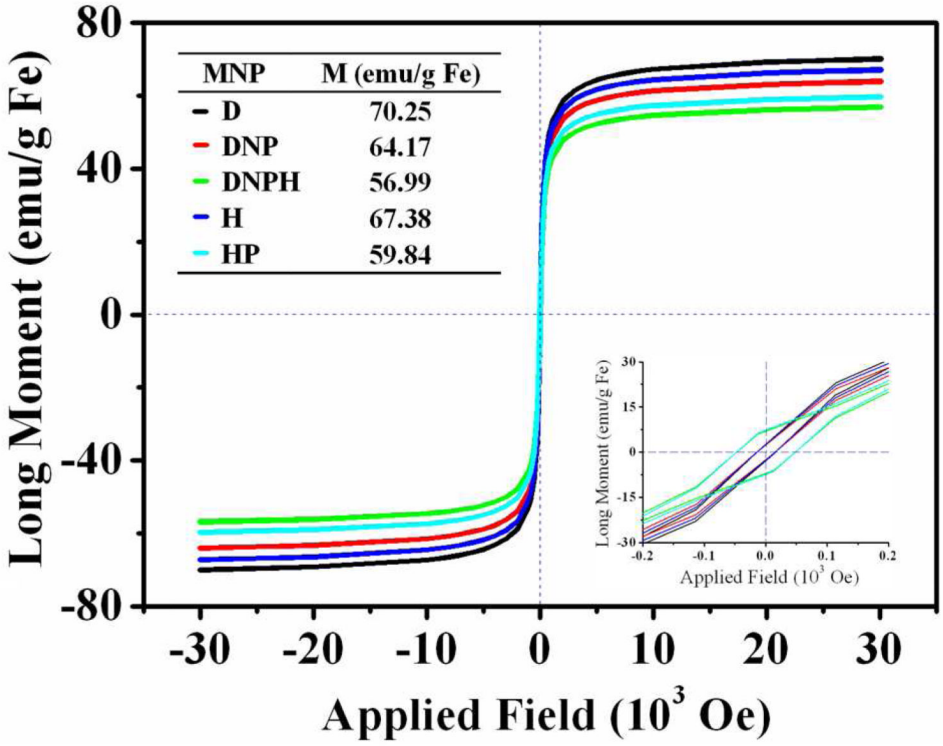

Figure 5.

Magnetization susceptibility of each MNP type. Inset image shows the data around zero field with an expanded scale. And inset table listed the saturation magnetization of each MNP type.

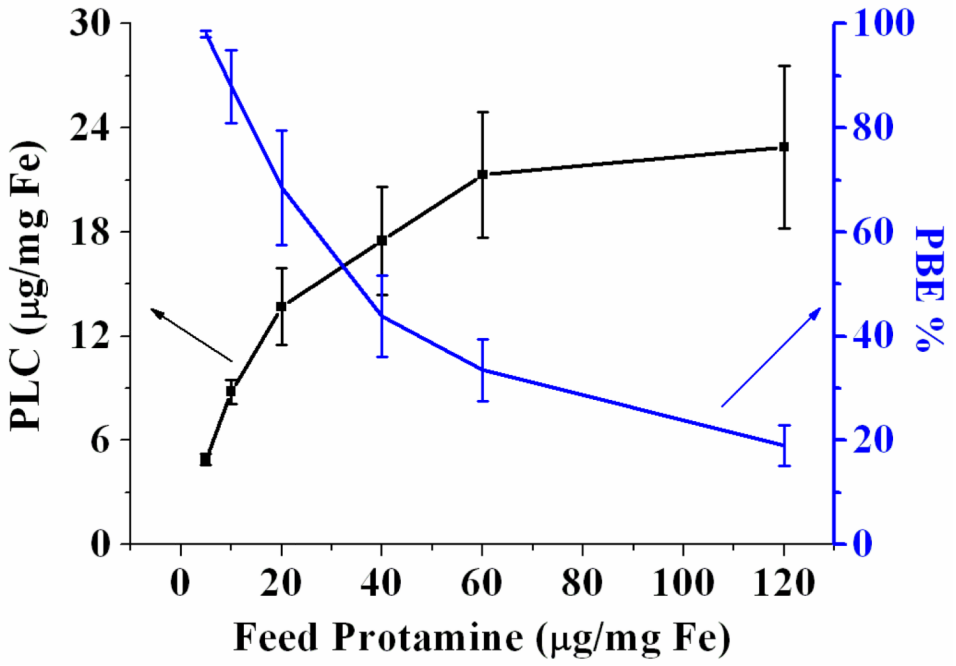

Figure 6.
Protamine loading content (PLC, black curve) and protamine binding efficiency (PBE, blue curve) on DNPH varied with the amount of feed protamine.

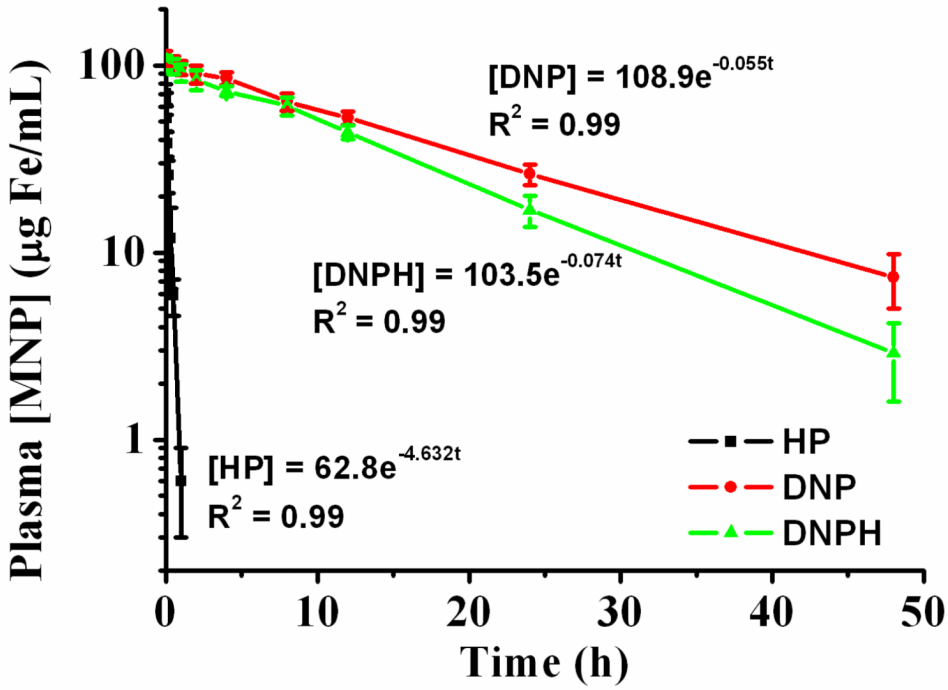

Figure 7.

Plasma pharmacokinetics of DNP, DNPH and HP in male C57BL6 black mouse (12 mg Fe/kg, ~ 20 g animal). Data for three kinds of MNP appeared to follow a one-compartment model and the model equation was shown next to each data set by applying a non-linear regression. Key pharmacokinetic parameters were extracted/calculated from models and shown in Table 2.

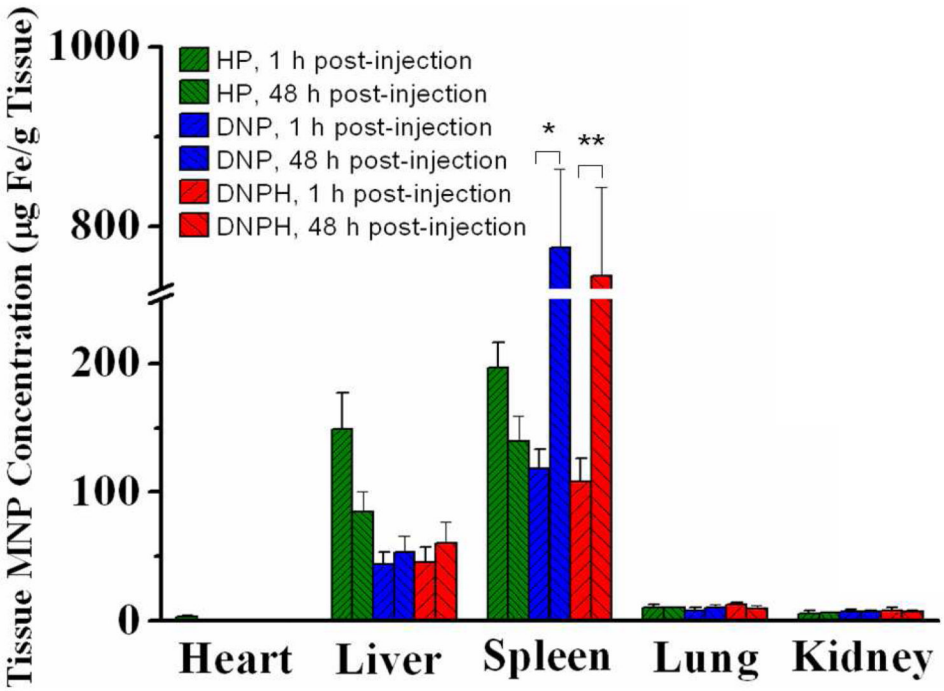

Figure 8.
Biodistribution of HP, DNP and DNPH in main organs (Heart, Liver, Spleen, Lung and Kidney) of mouse. (*,** = $p < 0.01$, determined by the Student t test).

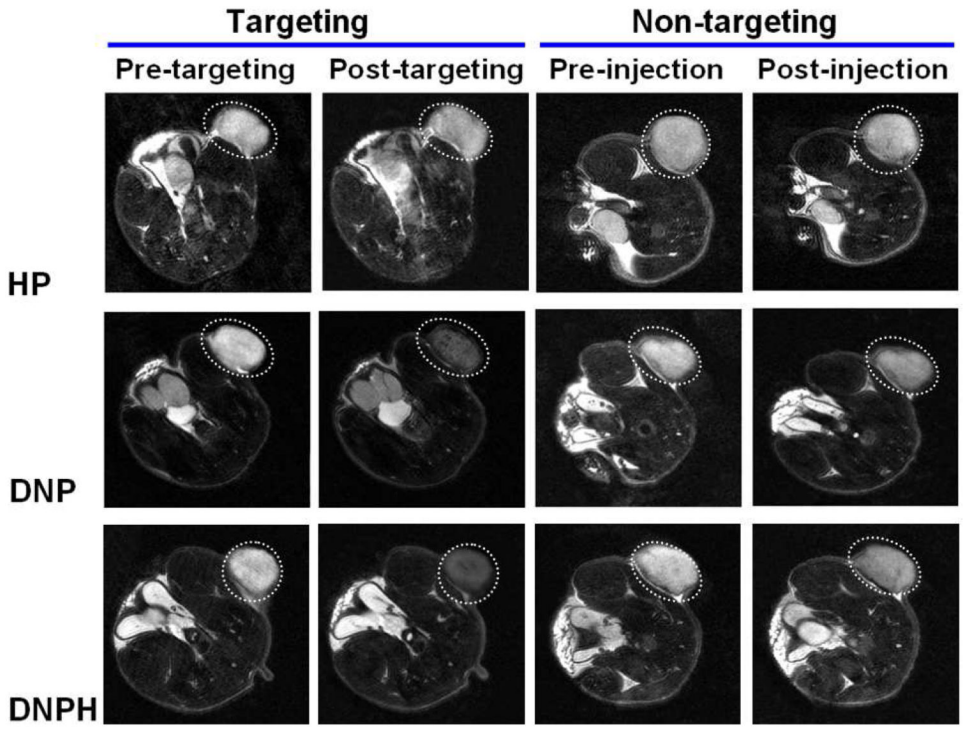

Figure 9.

Representative MRI images of mice bearing 9L-glioma flank tumors injected with HP, DNP or DNPH. For each MNP type, MRI images were taken prior to and at 60 min post-administration of MNP with/without magnetic targeting.

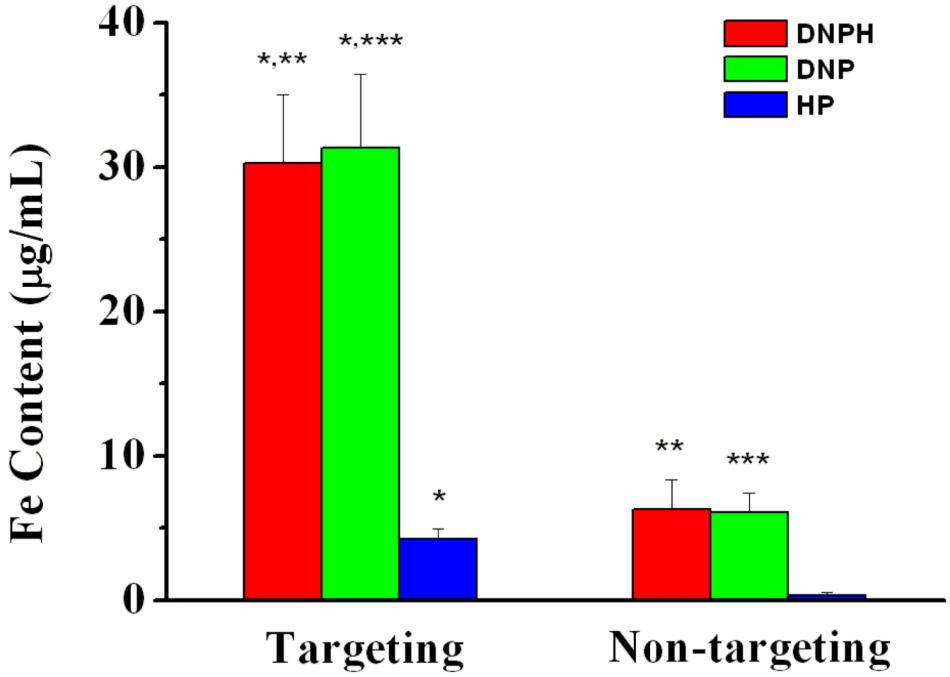

Figure 10.

Quantitative ESR analysis of MNP concentrations (Fe content) in targeted and no-targeted tumor tissues of mice administered with DNP, DNPH or HP. (*,**,*** = $p < 0.01$, determined by the Student t test).

Table 1

Characterization of D-based MNPs and H-based MNPs. “N/A” means measurement was not carried out.

MNP	Size distribution (nm)	Zeta Potential (mV)	[NH2] (nmol/mg Fe)	[PEG] μg/mg Fe	PEG/MNP (molecules/particle)	[Heparin] μg/mg Fe
D	104.7 ± 1.7	−4.4 ± 0.5	N/A	N/A	N/A	N/A
DN	136.3 ± 5.5	38.9 ± 3.2	278.1 ± 34.2	N/A	N/A	N/A
DNP	165.1 ± 8.2	23.8 ± 2.7	276.8 ± 31.1	25.6 ± 5.8	437 ± 97	N/A
DNPH	168.8 ± 9.9	−2.1 ± 0.7	N/A	N/D	N/D	35.4 ± 4.3
H	105.1 ± 2.2	−38.8 ± 3.3	N/A	N/A	N/A	N/D
HP	145.1 ± 7.9	−23.1 ± 3.7	N/A	24.6 ± 4.4	413	102.6 ± 3.5

“N/A”, not applicable; “N/D”, not determined.

Table 2

Calculated parameters of MNP in blood circulation obtained from experimentally determined pharmacokinetic model.

MNP	Co (μg Fe/mL)	K (1/h)	T1/2 (h)	Vd (mL/kg)	CL (mL/h/kg)	$AUC_{0-\infty}$ (μg Fe·h/mL)
HP	62.8	4.632	0.15	191.08	885.08	14
DNP	108.9	0.055	12.60	110.19	6.06	1957
DNPH	103.5	0.074	9.37	115.94	8.58	1490

Dose (20 g mouse) = 240 μg Fe. The parameters were defined as follow: C_O, the initial plasma Fe content; C(t), the plasma Fe content at time "t"; K, the elimination rate constant; $T_{1/2}$ (half-life), the time needed for 50% decrease of plasma Fe content; V_d, BW-normalized volume of distribution; CL, short for "clearance"; $AUC_{0-\infty}$, the total area-under-curve, indicating the total expected plasma MNP exposure per single dose.

Mol Pharm. Author manuscript; available in PMC 2014 October 07.